

## PAPER

# An Estimation Algorithm of Target Location and Scattered Waveforms for UWB Pulse Radar Systems

Takuya SAKAMOTO<sup>†</sup>, *Student Member* and Toru SATO<sup>†</sup>, *Member*

**SUMMARY** Radars utilizing ultra-wide-band (UWB) pulses are attractive as an environment measurement method for various applications including household robots. Suitable filtering is essential for accurate ranging, which requires an accurate waveform estimation. This paper presents a high-resolution algorithm of estimating target location and scattered waveforms, whose accuracies are interdependent. The technique relies on iterative improvements of estimated waveforms. Description of the algorithm is followed by statistical simulation examples. The performance of the algorithm is contrasted with conventional ones and statistical bounds. Results indicate that our proposed algorithm has a remarkable performance, which is close to the theoretical limit. Next, we clarify the problem of applying HCT to multiple targets. HCT for multiple targets can not be used as an estimated waveform because of interference waves from other targets. We propose an interference suppression algorithm based on a neural network, and show an application example of the algorithm.

**key words:** UWB pulse radar, radar imaging, waveform estimation, non-parametric estimation, neural network

## 1. Introduction

Radars utilizing ultra-wide-band (UWB) pulses have an advantage of directly measuring the range with high accuracies compared to other methods such as a technique with stereo cameras. They can also be used in situations where optical measurements are not available due to smoke in the scene of a fire or other hazardous areas. Therefore, a UWB pulse radar is attractive as an environment measurement method for various applications including household robots. However, the accuracy of a UWB pulse radar is not sufficient without a suitable filtering, which is a critical issue. Waveform estimation is very important for pulse radar systems because it improves locationing accuracies. Waveforms of scattered pulses are unknown without estimating target shape because scattered waveforms depend on the shape of the target. Therefore, it is required to estimate target locations and scattered waveforms simultaneously. In this paper, we propose an algorithm which simultaneously estimates target locations and scattered waveforms for UWB pulse radar systems [1].

Many kinds of imaging algorithms have been proposed [2]–[20]. Although parametric algorithms are effective approaches [2]–[14], they have problems concerning a calculation time and stabilities. On the other hand, non-parametric algorithms are helpful especially for DOA (Direction-Of-Arrival) estimation [15]–[20]. However, they can not be

used for target shape estimations. We have already developed a non-parametric shape estimation algorithm based on BST (Boundary Scattering Transform) [21]. The algorithm utilizes the existence of a reversible transform BST between target shapes and pulse delays. We extract quasi-wavefronts from observed data in the algorithm. Then, we obtain the target shape by applying the inverse BST to the quasi-wavefronts. The algorithm has a remarkable performance in estimating target shapes.

In this way, the algorithm works well and achieves a good estimation of target shapes, but a problem remains. The algorithm can not use an optimum filter because it does not estimate scattered waveforms. The difference between the scattered waveforms and the assumed waveforms degrades the estimation accuracy. Our objective is to develop a non-parametric high-resolution target locationing algorithm by improving the ranging accuracy iteratively. The algorithm should be applicable for a general situation including a near field and a far field. In this paper, we deal with an algorithm for locationing a point target for simplicity. Further studies are required to apply the proposed algorithm to the imaging algorithm based on BST.

In this paper, we propose a high-resolution estimation algorithm of target locations and scattered waveforms for UWB pulse radar systems. Firstly, we explain the algorithm and formulate the procedure. We then examine the performance of our method by contrasting it with conventional methods and statistical bounds using numerical simulations. Next, we clarify the problem of applying the proposed algorithm to multiple targets. We propose an algorithm of suppressing interference based on a neural network algorithm. Finally, we show an application example of the proposed interference suppression algorithm.

## 2. System Model

We assume an  $M$ -element linear sensor array with intervals of half-wavelength at the center frequency of the pulse, and one point target located within its near field. This is because it is more general and difficult to deal with a target in a near field rather than in a far field. We assume that each sensor is omni-directional and the effect of mutual coupling can be neglected. In the situation where these assumptions are not satisfied, we should compensate for the effects as discussed in Sec. 6. We transmit the pulse with the center sensor of the array, and receive the scattered signal with all the sensors. The received data with each sensor is input

Manuscript received July 10, 2003.

Manuscript revised October 29, 2003.

<sup>†</sup>The authors are with the Department of Communications and Computer Engineering, Graduate School of Informatics, Kyoto University, Kyoto-shi, 606-8501 Japan.

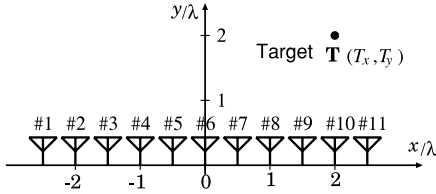


Fig. 1 The location of the sensor array and coordinates used in the present paper.

Table 1 Simulation parameters.

Sensor Array	$M = 11$
Sensor Interval	$0.5 \lambda$
IHCT Iteration	40 times
Observation Duration	$24 \lambda$
Sampling	83 samples/ $\lambda$

into an A/D converter, and stored into a memory. We define  $\mathbf{T} = [T_x, T_y]$  as the real target location. Figure 1 shows the location of the sensor array and the coordinates, where  $\lambda$  is the center wavelength of the transmitted signals. The transmitted pulse is a mono-cycle pulse, which is suitable for radar systems because it has no DC power. The used pulse has a relative bandwidth of 96.3%, which satisfies the condition of UWB determined by FCC (Federal Communications Commission) that UWB has a relative bandwidth of more than 20% of the carrier frequency, or an absolute bandwidth larger than 500 MHz. The scattered wave is a spherical wave because the target is within the near field. Therefore, the signal delay draws a hyperbola as a function of the location of the sensors. We assume that the observer has no information of scattered waveforms.

We deal with a 2-dimensional problem in this paper. We also define a signal image  $s(x, y)$  as

$$s((m - (M + 1)/2)d/\lambda, ct/\lambda) \equiv s'_m(t), \quad (1)$$

where  $s'_m(t)$  is the received signal with the  $m$ -th sensor,  $c$  is speed of the light, and  $d = \lambda/2$ . This definition of a signal image is advantageous because space  $x$  and time  $y$  are normalized by wavelength. Our algorithm estimates the target location  $\mathbf{T}$  using the signal image  $s(x, y)$ . Table 1 shows the simulation parameters.

### 3. Waveform and Filtering

In this section, we explain the importance of estimating waveforms in the proposed algorithm. Wiener filter is often used for estimation of the turn-around-time because it is an effective denoising filter. Wiener filter for signal  $G(\omega)$  is expressed as

$$W(\omega) = \frac{G^*(\omega)}{(1 - \eta) + \eta|G(\omega)|^2}, \quad (2)$$

where  $\eta = 1/(1 + (S/N)^{-1})$ .  $W(\omega)$  works as an inverse filter for large S/N ( $\eta \approx 1$ ). On the other hand, it works as a matched filter for small S/N ( $\eta \approx 0$ ). Here, we define the signal power  $S = \max |s(x, y)|^2$ .  $W(\omega)$  is the optimal filter,

in the sense that it minimizes the mean square error between the output signal and the impulse function. However, we can not directly apply Wiener filter to our purpose, because  $W(\omega)$  requires the scattered waveform  $G(\omega)$ . This is the reason why our proposed method is important.

### 4. Theoretical Limit of Locationing Accuracy

In this section we derive the theoretical limit for our problem. The derived theoretical limit is based on Cramer-Rao lower bound (CRLB) [22]. We define  $R_{\mathbf{T}-\mathbf{T}_i}$  as the covariance matrix of the estimation error of the target location, and  $\mathbf{T}_i = (x_i, y_i)$  as the estimated target location for  $i$ -th iteration. The original expression of CRLB is

$$R_{\mathbf{T}-\mathbf{T}_i} \geq J^{-1}(\mathbf{T}), \quad (3)$$

where  $J(\mathbf{T})$  is Fisher information matrix expressed as

$$J(\mathbf{T})_{j,k} = -E \left\{ \iint \frac{\partial^2 \log p(s|\mathbf{T})}{\partial T_j \partial T_k} dx dy \right\}, \quad (4)$$

where  $p(s|\mathbf{T})$  is the conditional probability density function of  $s(x, y)$  and  $j, k \in \{x, y\}$ . We define  $E\{\}$  as an expectation, which means an ensemble average. We can not directly use Eq. (3) because the estimation error is expressed as  $e_i = |\mathbf{T} - \mathbf{T}_i|$ . We thus define  $q(\Delta\mathbf{T})$  as the probability density function of  $\Delta\mathbf{T} = \mathbf{T} - \mathbf{T}_e$ , where  $\mathbf{T}_e$  is the theoretical best estimation. We assume  $q(\Delta\mathbf{T})$  as

$$q(\Delta\mathbf{T}) = \frac{(\det J(\mathbf{T}))^{1/2}}{2\pi} \exp \left[ -\frac{1}{2} \Delta\mathbf{T} J(\mathbf{T}) \Delta\mathbf{T}^T \right]. \quad (5)$$

Assuming Eq. (5) gives

$$e_i \geq e_{\text{CRLB}} = \int_{-\infty}^{\infty} |\Delta\mathbf{T}| q(\Delta\mathbf{T}) d\Delta\mathbf{T}. \quad (6)$$

$e_{\text{CRLB}}$  is the theoretical limit for the estimation of target location. We calculate  $e_{\text{CRLB}}$  for each S/N in order to contrast with the simulation results. We call  $e_{\text{CRLB}}$  as CRLB for simplicity in the following sections.

### 5. The Proposed Method for Locationing

In this section, we explain the proposed algorithm. We define Hyperbolic Coherent Transform (HCT) as

$$H(\omega, \mathbf{T}_i) \equiv \iint_{-\infty}^{\infty} s(x, y) \frac{e^{j\omega[u(x, \mathbf{T}_i) - y]}}{\sqrt{u(x, \mathbf{T}_i)}} dx dy, \quad (7)$$

where we define

$$u(x, \mathbf{T}_i) \equiv |\mathbf{T}_i| + \sqrt{(x - x_i)^2 + y_i^2}. \quad (8)$$

HCT works as the Fourier transform for  $y$ .  $u(x, \mathbf{T}_i)$  is a delay time compensation for  $x$ .  $\sqrt{u(x, \mathbf{T}_i)}$  is required in order to improve S/N of HCT, which we explain in the appendix. HCT estimates  $F(\omega)$ , which is the Fourier transform of the scattered waveform, using coherent integration of the received signals. We can describe the algorithm of target

location estimation as

$$\text{maximize}_{\mathbf{T}_{i+1}} \left| \int_{-\infty}^{\infty} \frac{H(\omega, \mathbf{T}_{i+1}) P_i^*(\omega)}{1 - \eta + \eta |P_i(\omega)|^2} d\omega \right|^2, \quad (9)$$

where  $P_i(\omega)$  is the waveform used for constructing Wiener filter. Equation (9) means to maximize the power of the filtered signal at  $t = 0$ , which is calculated in the frequency domain. This is based on the fact that substituting  $t = 0$  for  $\exp(j\omega t)$ , the integral kernel of the inverse Fourier transform, the integral kernel shrinks to 1. Equation (9) includes all algorithms we investigate in this paper, which depends on the definition of  $P_i(\omega)$ . We set the initial waveform  $H(\omega, \mathbf{T}_0)$  as the Fourier transform of the transmitted waveform. We optimize Eq. (9) using Quasi-Newton method, where we set the initial value of  $\mathbf{T}_i$  to the optimized  $\mathbf{T}_{i-1}$ . We determine the initial value of  $\mathbf{T}_1$  using a simple grid search.

We set  $P_i(\omega)$  to

$$P_i(\omega) = (H(\omega, \mathbf{T}_i) * \text{sinc}(t_0\omega)) |P_{i-1}(\omega)| \quad (10)$$

for the proposed algorithm. We call the proposed algorithm IHCT (Iterative HCT) because it is based on an iterative improvement of estimation. Equation (10) works as extraction of dominant-frequency waveform. The final form of  $P_i(\omega)$  is a narrow-band filter, which is apparently inferior to the ideal matched filter as a single filter for signal detection. However, the major problem of a narrow bandwidth is the ambiguity in finding the peak location, which is solved by the wide-band filter at earlier stages. A better resolution is obtained by accurately determining the phase of the dominant-frequency component. Convolution of  $\text{sinc}(t_0\omega)$  is a simple windowing, which prevents the waveform from having an extremely narrow band. We set  $t_0$  to the pulse duration of the transmitted signal. Figure 2 shows the outline of IHCT. We also define IHCTW (IHCT Without waveform estimation) which is a conventional method. We set  $P_i(\omega)$  for IHCTW as  $P_i(\omega) = H(\omega, \mathbf{T}_0)$ , which is the transmitted waveform. Moreover, we investigate IHCTK (IHCT with Known scattered waveform) which represents the ideal situation. We set  $P_i(\omega)$  for IHCTK as  $P_i(\omega) = F(\omega)$ , which is the true scattered waveform. IHCTK is not realistic because  $F(\omega)$  is unknown in an actual case. Table 2 shows  $P_i(\omega)$  for each method.

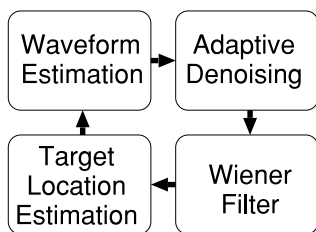


Fig. 2 The outline of IHCT.

Table 2  $P_i(\omega)$  (Denoised HCT) for each method.

IHCT	$(H(\omega, \mathbf{T}_i) * \text{sinc}(t_0\omega))  P_{i-1}(\omega) $
IHCTW	$H(\omega, \mathbf{T}_0)$
IHCTK	$F(\omega)$

## 6. Performance Evaluation of IHCT Algorithm

In this section we investigate the performance of the proposed method by contrasting with the conventional method and the theoretical limit. We assume the received waveform is the 1st order differential of the transmitted waveform. Figure 3 illustrates the waveform of  $P_i(\omega)$  for  $i = 1, 5$  and 10. The bandwidth of the waveform becomes narrower as the iteration proceeds.

Figure 4 shows the locating accuracy of each algorithm compared to CRLB. Here, we set the target location to  $\mathbf{T} = (2\lambda, 2\lambda)$ . The relationship between the estimation error  $e_L$  and the peak S/N is illustrated in the figure. IHCT, IHCTW and IHCTK have poor performance for  $S/N < 11$  dB due to invalid initial guess of  $\mathbf{T}_1$ , which is caused by the poor S/N. IHCTK achieves CRLB for  $S/N \geq 11$  dB, which means the optimization in Eq. (9) can achieve the theoretical limit only if we know the scattered waveform  $F(\omega)$ . IHCTW has a floor of estimation error for  $S/N \geq 11$  dB, which is caused by biases due to the fixed reference waveforms. The difference between the transmitted waveform and the scattered waveform causes this error. On the other hand, the performance of IHCT is close to CRLB. The ratio of the estimation accuracy of IHCT to that of CRLB is 1/4 at most. The estimation error of IHCT has no floor for  $S/N \leq 40$  dB. The estimation accuracy of IHCT is 140 times better than that of IHCTW. Moreover IHCT achieves an accuracy of  $10^{-3} \lambda$  for  $S/N > 34$  dB, which is sufficiently high for practical use.

Figure 5 shows the estimation error of target location

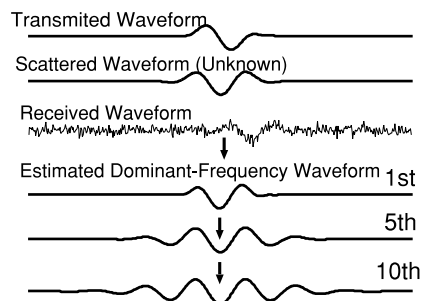


Fig. 3 Estimated dominant-frequency waveforms.

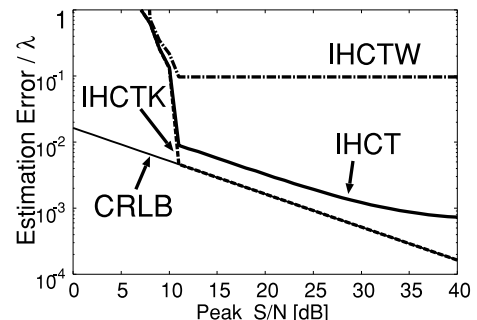


Fig. 4 Estimation error of the target location.

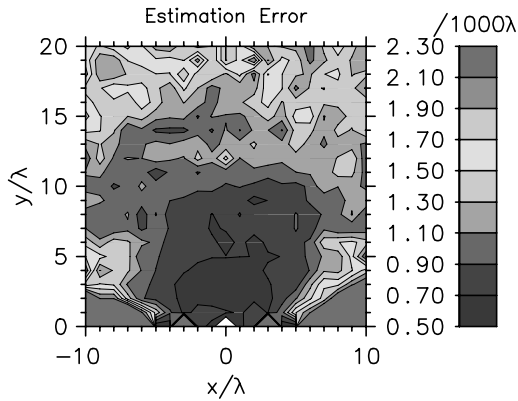


Fig. 5 Estimation error for various target locations.

using IHCT for various target locations for  $S/N = 40$  dB. From the figure, we see that the order of estimation error is  $10^{-3} \lambda$  for all target location except for the two areas on both sides of the array. The poor performance of IHCT in the two areas is caused by the ambiguity of the signal with target locations.

In actual case, the effect of mutual coupling may not be neglected. In such a case, it is possible to compensate for the pattern of mutual coupling because IHCT is based on iterative improvement. The compensation factor can be calculated using the target location estimated at each iteration. We have confirmed the validity of the compensation algorithm of mutual coupling implemented in the IHCT algorithm for a case where the gain varies by 1 dB.

We have proposed a locationing algorithm for UWB pulses. If it is applied to narrow-band signals, the resolution degrades because it is difficult to determine the initial value because of the ambiguity due to periodicity of narrow-band signals. We have shown the application example of the algorithm for a target in a near field. However, the proposed algorithm can be applied for a far field as well. As for computational time, the proposed algorithm with iteration of 40 times takes about 50 sec with Xeon 2.8 GHz processor.

## 7. Interference Suppression Algorithm for HCT of Multiple Targets

An accurate locationing of targets requires an accurate waveform estimation as described in the previous sections. HCT for a single target can be used as an estimation of the waveform although the noise reduction algorithm is needed. On the other hand, HCT for multiple targets can not be used as a waveform estimation due to the problem of interference. The waveform scattered by a certain target is integrated coherently, and the waveforms scattered by other targets are summed with random delays, which causes cancellation of waves. However, the cancellation of interference waves is not sufficient because the number of antennas is limited, and the signal power is localized. Interference waves can not be neglected especially if the number of targets is large. This residual interference wave is one of the most critical prob-

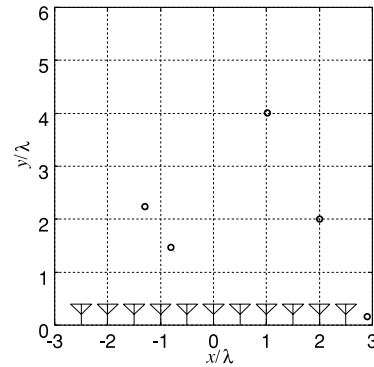


Fig. 6 Multiple targets location and antennas.

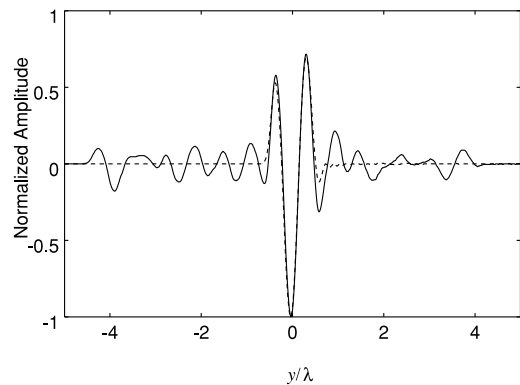


Fig. 7 HCT for multiple targets and true waveform for  $s(x, y)$ .

lems when HCT is applied to multiple targets. In this section, we propose an interference suppression algorithm for HCT. We also show the application example of the proposed algorithm using a numerical simulation.

Firstly, we show an example of interference waves. We assume that 5 point targets are located as symbols in Fig. 6. Each waveform of the target is the 1st order differential of the transmitted waveform. We assume that we do not have any information about the scattered waveform. We define  $h(y, T)$  as the IFT (Inverse Fourier Transform) of  $H(\omega, T)$ , and we deal with HCT in the time domain. In Fig. 7, the broken line indicates the true scattered waveform, and the solid line indicates  $h(y, T)$  for  $T = (2\lambda, 2\lambda)$ . In the figure, we see that undesirable interference waves exist in HCT.

We define  $\sigma(y)$  as a standard deviation of waveforms, which is expressed as

$$\sigma(y) = A_\sigma \sqrt{\int_{-\infty}^{\infty} s(x, y)^2 dx}, \quad (11)$$

where we set  $A_\sigma$  to satisfy  $\max \sigma(y) = 1$ . We also define  $e(y)$  as the instantaneous envelope [23] of HCT.  $e(y)$  can be expressed as

$$e(y) = A_e \left| h(y, T) + \frac{j}{\pi} \int_{-\infty}^{\infty} \frac{h(v, T)}{y - v} dv \right|, \quad (12)$$

where we set  $A_e$  to satisfy  $\max e(y) = 1$ . The integration in Eq. (12) means Hilbert Transform of  $h(y, T)$ . Figure 8

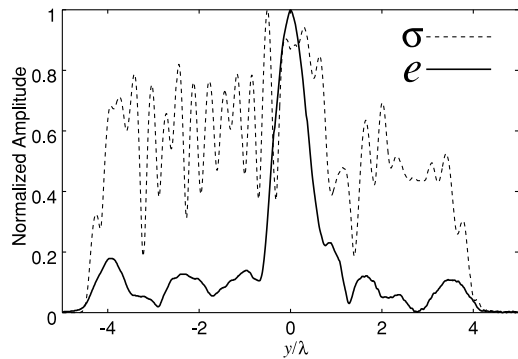


Fig. 8  $\sigma(y)$  and  $e(y)$  for  $s(x, y)$ .

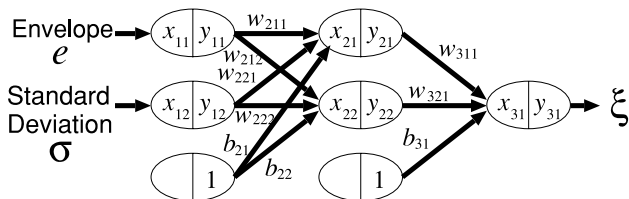


Fig. 9 Neural network model utilized in the proposed algorithm.

shows  $\sigma(y)$  and  $e(y)$  for the observed data. In the figure, we see that  $\sigma(y)$  is small compared to  $e(y)$  where the true wave exists. We propose an interference suppression algorithm by utilizing this characteristic. We define an interference-suppressed waveform  $\hat{h}(y, T)$  as

$$\hat{h}(y, T) = \xi(\sigma(y), e(y)) h(y, T), \tag{13}$$

where  $\xi(\sigma, e)$  is a weight function. We select  $\xi(\sigma, e)$  to satisfy

$$\text{minimize}_{\xi} \int_{-\infty}^{\infty} \{\hat{h}(y, T) - f(y)\}^2 dy, \tag{14}$$

where  $f(y)$  is the IFT of  $F(\omega)$ , which is the true scattered waveform. We utilize a neural network in order to optimize  $\xi(\sigma, e)$  because  $\xi(\sigma, e)$  should be dealt with as a nonlinear function in general. We utilize a 3-layered neural network shown in Fig. 9. The ellipse symbols in the figure indicate sigmoid functions. We define  $x_{m,n}$  and  $y_{m,n}$  as the  $n$ -th values in the  $m$ -th layer.  $y_{m,n}$  are calculated as

$$y_{m,n} = u(x_{m,n}) \tag{15}$$

$$= 1 / \{1 + \exp(-x_{m,n})\}, \tag{16}$$

where  $u(x)$  is called a sigmoid function.  $x_{m,n}$  are calculated as

$$x_{m,n} = \sum_{l=1}^L w_{m,l,n} y_{m-1,l} + \beta_{m,n}, \tag{17}$$

where, we set  $L = 2$ . Figure 10 shows the procedure of suppressing interference in the proposed algorithm, assuming the parameters in the neural network is already optimized. In order to obtain the solution of the minimization problem in Eq. (14), it is required to know the true scattered waveform  $f(y)$ . Here, it is impossible to know  $f(y)$  prior to the

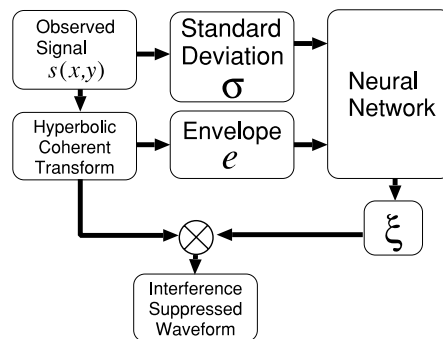


Fig. 10 The outline of interference suppression in the proposed algorithm.

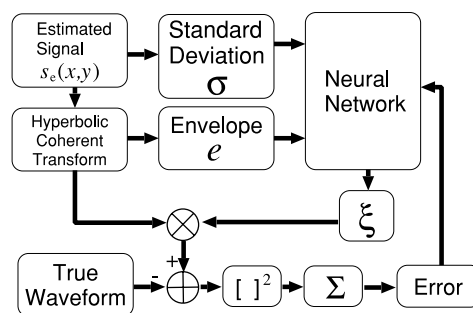


Fig. 11 The outline of neural network learning procedure in the proposed algorithm.

waveform estimation. Therefore, in the proposed algorithm, we utilize the transmitted waveform  $h(y, T_0)$  instead of the true scattered waveform  $f(y)$ . We assume that we know approximate locations of the targets.

The proposed algorithm for an interference suppression is as follows. Firstly, we generate an estimated received signal  $s_e(x, y)$  assuming all the signals from targets are equal to  $h(y, T_0)$ . Then, we calculate  $e(y)$  and  $\sigma(y)$  from  $s_e(x, y)$ . In this case, we can solve the minimization problem in Eq. (14) because we know the true waveform  $h(y, T_0)$ . We determine the function  $\xi(\sigma, e)$  by solving the optimization problem with  $e(y)$ ,  $\sigma(y)$  and  $h(y, T_0)$  for  $s_e(x, y)$ . Figure 11 shows the outline of learning procedure with the neural network in the proposed algorithm. The sum of the error in the figure is minimized for  $s_e(x, y)$ . We utilize Levenberg-Marquardt-Morrison method for this optimization. Next, we calculate  $e(y)$  and  $\sigma(y)$  for  $s(x, y)$ . Then we calculate an interference-suppressed waveform for  $s(x, y)$  as in Fig. 10. In this way, we obtain waveform  $\hat{h}(y, T)$  after the interference suppression.

We show an application example of the proposed algorithm. In Fig. 12, the broken line and the solid line indicate  $h(y, T_0)$  and  $h(y, T)$  for  $s_e(x, y)$ , respectively. The interference waveform in the figure is completely different from that of  $s(x, y)$  in Fig. 7. Figure 13 shows  $e(y)$  and  $\sigma(y)$  calculated for  $s_e(x, y)$ . We solve the optimization problem in Eq. (14) and determine the function  $\xi(\sigma, e)$ . Then, we obtain  $\hat{h}^*(y, T)$  for  $s_e(x, y)$ . The solid line and broken line in Fig. 14 show

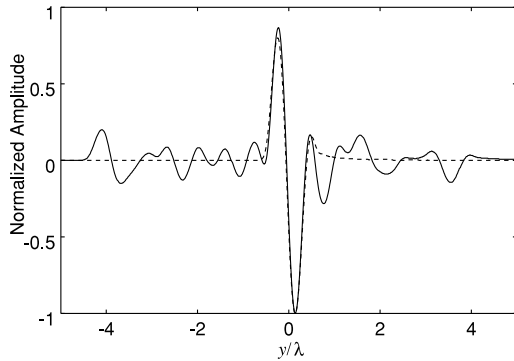


Fig. 12 HCT for multiple targets and true waveform for  $s_e(x, y)$ .

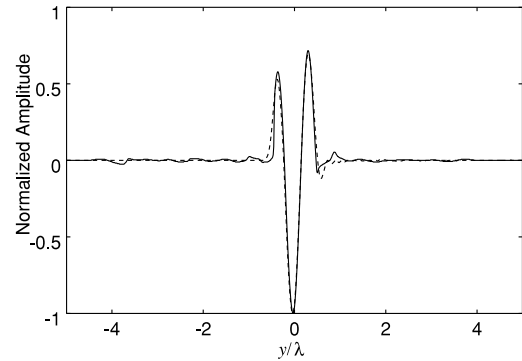


Fig. 15 Interference suppressed waveform and true waveform for  $s(x, y)$ .

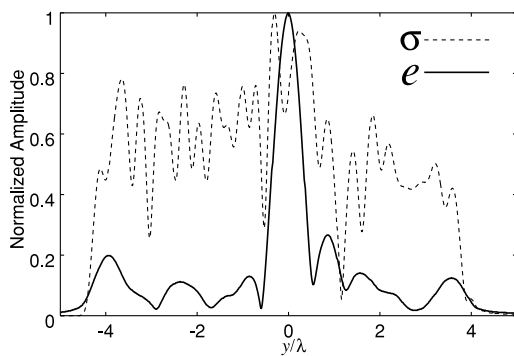


Fig. 13 Instantaneous envelope of HCT and standard deviation using  $s_e(x, y)$ .

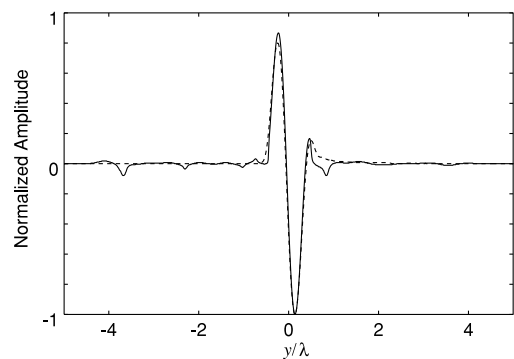


Fig. 14 Interference suppressed waveform and true waveform for  $s_e(x, y)$ .

$\hat{h}^*(y, \mathbf{T})$  and  $h(y, \mathbf{T}_0)$  respectively. We see that  $\xi(\sigma, e)$  can suppress the interference waves to  $s_e(x, y)$ . Next, we multiply  $h(y, \mathbf{T})$  by  $\xi(\sigma, e)$  in order to suppress the interference of  $s(x, y)$ . In Fig. 15, the solid line and the broken line show the interference-suppressed waveform  $\hat{h}(y, \mathbf{T})$  and the true waveform  $f(y)$  for  $s(x, y)$  respectively. In the figure, we see that the proposed algorithm successfully suppresses the interference for  $s(x, y)$ .

As a result, we clarified that the proposed algorithm has a sufficient performance in suppressing interference waves. Accurate estimations can be accomplished not only for  $s_e(x, y)$  but also for  $s(x, y)$ . Although the function  $\xi(\sigma, e)$

is optimized for  $s_e(x, y)$ , it works well for  $s(x, y)$ . The learning procedure of the neural network in the proposed algorithm can be accomplished without the true waveforms, because  $\xi(\sigma, e)$  depends only on the amplitude distributions of  $e(y)$  and  $\sigma(y)$  and the true waveform. It should be noted that the proposed algorithm selects strong signals regardless of whether they are from desired or undesired targets. We thus assume that the interference waves have comparatively small power because the signals with large power are chosen firstly.

## 8. Conclusions

UWB pulse radar systems are promising candidates for environment measurement. Firstly, we proposed a high-resolution algorithm for target locating without information of scattered waveforms. The proposed method simultaneously estimates target locations and scattered waveforms for UWB pulse radar systems. The proposed method estimates dominant-frequency waveforms of scattered waveform iteratively. We also examined the performance of our method by contrasting them with conventional methods and statistical bounds. We evaluated the performance in terms of the estimation accuracy of target locations utilizing numerical simulations. We showed that the performance of the proposed method is close to the theoretical limit. We clarified that the estimation accuracy of the proposed method is 140 times better than that of the conventional method. We also made it clear that the proposed method achieves an accuracy of  $10^{-3} \lambda$  for  $S/N > 34$  dB.

Next, we proposed an interference suppression algorithm for HCT. Interference waves in HCT can not be neglected especially if the number of targets is large. This residual interference wave is one of the most critical problems when HCT is applied to multiple targets. The proposed algorithm optimizes a weight function, whose variables are the instantaneous envelope of HCT and the standard deviation of waveforms. The proposed algorithm optimizes the weight function by utilizing the transmitted waveform instead of the scattered waveform. We showed an application example of the proposed algorithm, and clarified that the proposed algorithm has a sufficient performance in

suppressing interference waves. Further studies are needed in order to apply the interference suppression algorithm to IHCT, which leads to a high-resolution locationing algorithm for multiple targets.

In this paper, we have investigated the performance of the proposed algorithm only with numerical simulations. An experimental confirmation of the performance of the algorithm will be an important future task.

### Acknowledgment

This work is supported in part by the 21st Century COE Program (Grant No. 14213201).

### References

- [1] T. Sakamoto and T. Sato, "An estimation method of target location and scattered waveforms for UWB pulse radar systems," Proc. 2003 IEEE International Geoscience and Remote Sensing Symposium, pp.4013–4015, Toulouse, France, 2003.
- [2] J.V. Candy and C. Pichot, "Active microwave imaging: A model-based approach," IEEE Trans. Antennas Propag., vol.39, no.3, pp.285–290, 1991.
- [3] P. Chaturvedi and R.G. Plumb, "Electromagnetic imaging of underground targets using constrained optimization," IEEE Trans. Geosci. Remote Sens., vol.33, no.3, pp.551–561, 1995.
- [4] T. Sato, K. Takeda, T. Nagamatsu, T. Wakayama, I. Kimura, and T. Shinbo, "Automatic signal processing of front monitor radar for tunnelling machines," IEEE Trans. Geosci. Remote Sens., vol.35, no.2, pp.354–359, 1997.
- [5] T. Sato, T. Wakayama, and K. Takemura, "An imaging algorithm of objects embedded in a lossy dispersive medium for subsurface radar data processing," IEEE Trans. Geosci. Remote Sens., vol.38, no.1, pp.296–303, 2000.
- [6] W.C. Chew and Y.M. Wang, "Reconstruction of two dimensional permittivity distribution using the distorted Born iterative method," IEEE Trans. Med. Imaging, vol.9, no.2, pp.218–225, 1990.
- [7] M. Moghaddam and W.C. Chew, "Study of some practical issues in inversion with the Born iterative method using time-domain data," IEEE Trans. Antennas Propag., vol.41, no.2, pp.177–184, 1993.
- [8] G.P. Otto and W.C. Chew, "Microwave inverse scattering—Local shape function imaging for improved resolution of strong scatterers," IEEE Trans. Microw. Theory Tech., vol.42, no.1, pp.137–142, 1994.
- [9] H. Harada, D. Wall, T. Takenaka, and M. Tanaka, "Conjugate gradient method applied to inverse scattering problem," IEEE Trans. Antennas Propag., vol.43, no.8, pp.784–792, 1995.
- [10] A.E. Yagle and J.L. Frolik, "On the feasibility of impulse reflection response data for the two-dimensional inverse scattering problem," IEEE Trans. Antennas Propag., vol.44, no.12, pp.1551–1564, 1996.
- [11] A. Franchois and C. Pichot, "Microwave imaging—Complex permittivity reconstruction with a Levenberg-Marquardt method," IEEE Trans. Antennas Propag., vol.45, no.2, pp.203–215, 1997.
- [12] C. Chiu and W. Chen, "Electromagnetic imaging for an imperfectly conducting cylinder by the genetic algorithm," IEEE Trans. Microw. Theory Tech., vol.48, no.11, pp.1901–1905, 2000.
- [13] T. Takenaka, H. Jia, and T. Tanaka, "Microwave imaging of an anisotropic cylindrical object by a forward-backward time-stepping method," IEICE Trans. Electron., vol.E84-C, no.12, pp.1910–1916, Dec. 2001.
- [14] C. Chiu, C. Li, and W. Chan, "Image reconstruction of a buried conductor by the genetic algorithm," IEICE Trans. Electron., vol.E84-C, no.12, pp.1946–1951, Dec. 2001.
- [15] R.O. Schmidt, "Multiple emitter location and signal parameter estimation," IEEE Trans. Antennas Propag., vol.AP-34, no.3, pp.276–280, 1988.
- [16] H. Hung and M. Kaveh, "Focussing matrices for coherent signal-subspace processing," IEEE Trans. Acoust., Speech Signal Process., vol.36, no.8, pp.1272–1282, 1988.
- [17] S. Sivanand, J. Yang, and M. Kaveh, "Focusing filters for wide-band direction finding," IEEE Trans. Signal Process., vol.39, no.2, pp.437–445, 1991.
- [18] T. Sato, "Shape estimation of space debris using single-range doppler interferometry," IEEE Trans. Geosci. Remote Sens., vol.37, no.2, pp.1000–1005, 1999.
- [19] J.C. Chen, R.E. Hudson, and K. Yao, "Maximum-likelihood source localization and unknown sensor location estimation for wideband signals in the near-field," IEEE Trans. Signal Process., vol.50, no.8, pp.1843–1854, 2002.
- [20] D. Nahamoo, S.X. Pan, and A.C. Kak, "Synthetic aperture diffraction tomography and its interpolation-free computer implementation," IEEE Trans. Sonics Ultrason., vol.31, no.4, pp.218–229, 1984.
- [21] T. Sakamoto and T. Sato, "A target shape estimation algorithm for pulse radar systems based on boundary scattering transform," IEICE Trans. Commun., vol.E87-B, no.5, pp.1357–1365, May 2004.
- [22] C.R. Rao, Linear Statistical Inference and Its Applications, 2nd ed., Wiley, New York, 1973.
- [23] L. Cohen, "Time-frequency distributions—A review," Proc. IEEE, vol.77, pp.941–981, 1989.

### Appendix: Optimum Signal Processing for Coherent Integrations

We define data vector  $X(\omega)$  as

$$X(\omega) = \begin{bmatrix} S(\omega) + N_1(\omega) \\ S(\omega) + N_2(\omega) \\ \vdots \\ S(\omega) + N_M(\omega) \end{bmatrix}, \quad (\text{A} \cdot 1)$$

where  $S(\omega)$  is a signal, and  $N_i(\omega)$  are white Gaussian noises independent of one another.

We define  $W(\omega)$  as a Wiener filter which output the Dirac delta function  $\delta(t)$ . We also define  $S_{ab}$  as the covariance matrices between  $a$  and  $b$ , where  $a$  and  $b$  are given matrices. For example,  $S_{ab} = E\{a^T(\omega)b(\omega)\}$ . We can express  $W(\omega)$  as

$$\begin{aligned} W(\omega) &= S_{xx}^{-1}(\omega) S_{xx}^{-1}(\omega) \\ &= \begin{bmatrix} E\{1(S(\omega) + N_1(\omega))^*\} \\ E\{1(S(\omega) + N_2(\omega))^*\} \\ \vdots \\ E\{1(S(\omega) + N_M(\omega))^*\} \end{bmatrix} \\ &\quad \cdot S_{xx}^{-1}(\omega). \end{aligned} \quad (\text{A} \cdot 2)$$

Here, we define

$$A = \text{diag}\{\sigma_1^2, \sigma_2^2, \dots, \sigma_N^2\}, \quad (\text{A} \cdot 4)$$

$$v = \begin{bmatrix} S(\omega) & \dots & S(\omega) \end{bmatrix}^T. \quad (\text{A} \cdot 5)$$

Then, we can express  $W(\omega)$  as

$$W(\omega) = S^*(\omega) \begin{bmatrix} 1 \\ 1 \\ \vdots \\ 1 \end{bmatrix}$$

$$\cdot \left\{ A + |S(\omega)|^2 \begin{bmatrix} 1 & \cdots & 1 \\ \vdots & \ddots & \vdots \\ 1 & \cdots & 1 \end{bmatrix} \right\}^{-1} \quad (\text{A}\cdot 6)$$

$$= S^*(\omega) \begin{bmatrix} 1 \\ 1 \\ \vdots \\ 1 \end{bmatrix} \{A + \mathbf{v}\mathbf{v}^H\}^{-1} \quad (\text{A}\cdot 7)$$

By applying the following formula for matrix inversion

$$(A + \mathbf{v}\mathbf{v}^H)^{-1} = A^{-1} - \frac{A^{-1}\mathbf{v}\mathbf{v}^HA^{-1}}{1 + \mathbf{v}^HA^{-1}\mathbf{v}} \quad (\text{A}\cdot 8)$$

to Eq. (A·7), we obtain

$$W(\omega) = \frac{1}{\sum_{j=1}^M \sigma_j^{-2} |S(\omega)|^2 + \left( \sum_{j=1}^M \sigma_j^{-2} \right)^{-1}} \frac{S^*(\omega)}{\begin{bmatrix} \sigma_1^{-2} \\ \sigma_2^{-2} \\ \vdots \\ \sigma_M^{-2} \end{bmatrix}} \quad (\text{A}\cdot 9)$$

And thus, we see the optimum signal processing require a weight in proportion to each signal power. This is the reason why we need a term  $1/\sqrt{u(x, \mathbf{T}_i)}$  in Eq. (7).



**Takuya Sakamoto** received the B.E. degree in electrical engineering from Kyoto University, Kyoto, Japan in 2000, the M.I. degree in informatics from Graduate School of Informatics, Kyoto University in 2002. He is currently studying for the Ph.D. degree in informatics at Graduate School of Informatics, Kyoto University. His current research interest is in digital signal processing. He is a member of the IEEE.



**Toru Sato** received his B.E., M.E., and Ph.D. degrees in electrical engineering from Kyoto University, Kyoto, Japan in 1976, 1978, and 1982, respectively. He has been with Kyoto University since 1983 and is currently a Professor in the Department of Communications and Computer Engineering, Graduate School of Informatics. His major research interests have been system design and signal processing aspects of atmospheric radars, radar remote sensing of the atmosphere, observations of precipitation using radar and satellite signals, radar observation of space debris, and signal processing for subsurface radar signals. Dr. Sato was awarded Tanakadate Prize in 1986. He is a member of the Society of Geomagnetism and Earth, Planetary and Space Sciences, the Japan Society for Aeronautical and Space Sciences, the Institute of Electrical and Electronics Engineers, and the American Meteorological Society.

Dr. Sato was awarded Tanakadate Prize in 1986. He is a member of the Society of Geomagnetism and Earth, Planetary and Space Sciences, the Japan Society for Aeronautical and Space Sciences, the Institute of Electrical and Electronics Engineers, and the American Meteorological Society.